



TITLE:

Studies on the Flow Patterns of Liquids in a Cylindrical Mixing Vessel, Over a Wide Range of Reynolds Number

AUTHOR(S):

NAGATA, Shinji; YAMAMOTO, Kazuo; HASHIMOTO, Kenji; NARUSE, Yūji

CITATION:

NAGATA, Shinji ...[et al]. Studies on the Flow Patterns of Liquids in a Cylindrical Mixing Vessel, Over a Wide Range of Reynolds Number. Memoirs of the Faculty of Engineering, Kyoto University 1960, 22(1): 68-85

ISSUE DATE:

1960-03-10

URL:

<http://hdl.handle.net/2433/280460>

RIGHT:

Studies on the Flow Patterns of Liquids in a Cylindrical Mixing Vessel, Over a Wide Range of Reynolds Number

By

Shinji NAGATA*, Kazuo YAMAMOTO*, Kenji HASHIMOTO*
and Yūji NARUSE*

(Received October 23, 1959)

The flow patterns of liquids agitated in a cylindrical mixing vessel without baffles were measured by a photographic method, ranging from laminar to so-called transitional flow.

The authors are now able to discuss the flow pattern of the liquid and the discharge performance of the impellers over a wide range of Reynolds number, combined with the previous results published for the turbulent flow range¹⁾.

Some of the experimental results are shown in **Figs. 6, 7, 8 and 10.**

The authors discovered the following results on the velocity distribution of the liquid :

In the range of very small Reynolds number, the liquid velocity is considerably high only in the neighbourhood of the impeller and decreases abruptly with the distance from the impeller. On the other hand, in the range of high Reynolds number, secondary circulation flow occurs as shown in **Fig. 9** and also the flow becomes turbulent, so that the liquid attains considerable velocity even at a distance from the impeller by the transmission of momentum, and the velocity distribution is considerably unified throughout the vessel.

Concerning the discharge flow from the tip of the impeller blades which causes the secondary circulation, the non-dimensional quantities, N_{q_1} , and N_P/N_{q_1} , are defined, as in the previous report¹⁾. These values were calculated and the characteristic curves of discharge performance were obtained for various types of impellers (refer to **Table 1**), as shown in **Fig. 12.**

Furthermore, the relations between flow pattern, discharge performance and power consumption (N_P-Re relation) were discussed.

I. Introduction

The flow patterns of liquids agitated in a cylindrical mixing vessel in the turbulent-flow range have already been measured by the authors using pitot-tubes¹⁾, but little information is now available concerning the liquid flow patterns in the range of low Reynolds number.

Now, it is desirable to determine the flow pattern of the liquid and the discharge performance of the impellers over a wide range on Reynolds number, as has already been done concerning the power consumption of impellers.

* Department of Chemical Engineering

The flow patterns of the agitated liquid were measured, ranging from laminar to so-called transitional flow. And, combined with the knowledge of the flow pattern in the turbulent flow range, a general discussion of the flow patterns and the characteristics of impellers is offered.

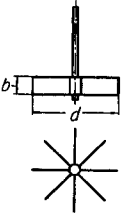
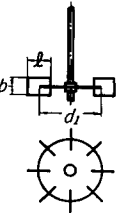
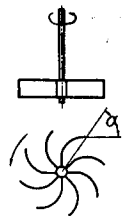
II. Equipment Used and Method of Measurement

In order to measure the flow patterns of an agitated liquid in the lower range of Reynolds number, a highly viscous and transparent newtonian liquid, such as millet-jelly, was used as the agitated liquid. As it is difficult to use pitot-tubes for the measurement of the flow velocity of highly viscous liquids, some other method had to be used. Hot-wire anemometry was attempted, but it was not successful. Finally, a photographic method was adopted, that is, a plane beam of light is projected through various sections of the agitated liquid containing a suspension of fine particles, such as sieved naphthalene powder, which move about with the fluid and reflect light when in the illuminated section. Photographs of the trajectories of the gleaming particles show the flow patterns of the agitated liquid. This method is similar to that used by J. P. Sachs and J. H. Rushton², who measured the flow patterns of agitated liquids in the turbulent flow range.

1) Equipment Used and Principles of Measurement

Three typical impellers were used as shown in Table 1, that is, impellers of the flat-blade-paddle type, turbine type and retreated-blade-paddle type, and the

Table 1. Various Types of Impellers Used.

(C) $\frac{\delta}{2}$ -Flat-Blade Paddle	(B) $\frac{\delta}{2}$ -Flat-Blade Turbine	(A) $\frac{\delta}{2}$ -Retreated-Blade Paddle
		
$\left\{ \begin{array}{l} n_p = 8 \\ d = 15 \text{ cm} \\ b = 3 \text{ cm} \end{array} \right.$	$\left\{ \begin{array}{l} n_p = 8 \\ d = 15 \text{ cm} \\ b = 3 \text{ cm} \\ d_1 = 11.3 \text{ cm} \\ l = 3.75 \text{ cm} \end{array} \right.$	$\left\{ \begin{array}{l} n_p = 8 \\ d = 15 \text{ cm} \\ b = 3 \text{ cm} \\ \alpha = 60^\circ \end{array} \right.$

conditions of their installation are shown in Fig. 1. The mixing vessel used is a cylindrical vessel geometrically similar to that used in the previous report¹, and made of transparent vinyl-chloride. It has a diameter of 30 cm and is filled with transparent millet-jelly to a depth equal to the diameter, and an agitating impeller is set along the central axis of the vessel at the midpoint of the liquid depth. The vertical position is represented by the height (z) from the midpoint of the liquid depth and

the radial position by the distance (r) from the agitator axis, as shown in Fig. 1 (b). The properties of the agitated liquid used (transparent millet-jelly diluted with tap water) and the light-reflecting particles (sieved naphthalene powder) are shown in Table 2.

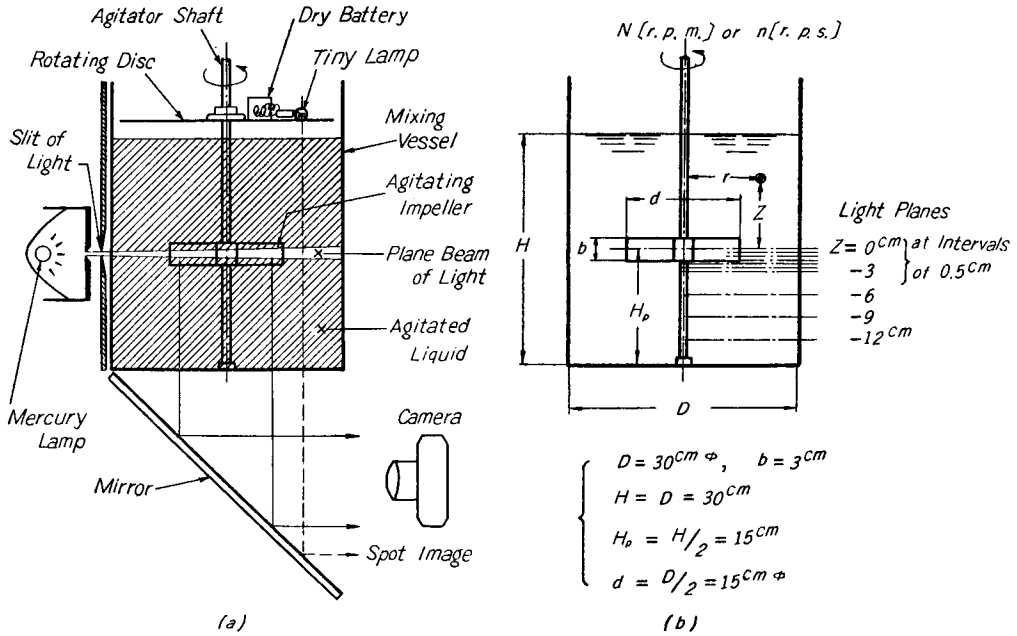


Fig. 1. Experimental Apparatus.

The liquid velocity is resolved, as shown in Fig. 2, into its vertical, radial and circumferential (tangential) components, v_z , v_r , and v_t respectively. Therefore, in order to measure the three components, the trajectories of the gleaming particles must be photographed both in the horizontal plane (represented by the “Z-view” in Fig. 2) and in the vertical plane containing the agitator axis (the “R-view” in Fig. 2). From the trajectories on the photograph of the Z-view, the tangential and radial components of the liquid velocity are obtained and from the trajectories on the photograph of the R-view, the vertical and radial velocities are obtained.

In Fig. 1 (a), the agitation vessel is immersed in a transparent and rectangular

Table 2. Agitated Liquid and Tracer Particles.
Agitated Liquid: Millet Jelly

Symbol	Temperature	Viscosity	Density
A	14~15°C	17.5~16 poise	1.35
B	7~17°C	12 ~ 6 poise	1.33
C	10~20°C	0.6~ 0.3 poise	1.22

Tracer Particles; Naphthalene Powder
Size: 20~28 mesh (0.59~0.83 mm)
Specific Weight: 1.15

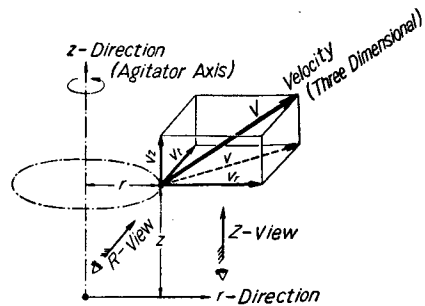


Fig. 2. Velocity and its Components.

aquarium filled with tap water and covered with black sheets, and a stream of light from a high-pressure mercury lamp is confined to a plane sheet of 3~5 mm width by means of the two slit barriers and is projected through a section of the agitated liquid in question. Actually, it is difficult to measure the vertical velocity of liquid v_z by the photograph of the R -view, because the magnitude of v_z is much smaller than v_t or v_r . Consequently, the measurements were limited to the radial and tangential velocities (v_r and v_t) in this experiment. The rotating-disc attached to the agitator axis has a pin-hole, through which the light from a tiny lamp forms a spot-light and marks a trajectory of a circular arc on the photograph. This arc length corresponds of the length of time of exposure for the photograph.

2) Method of Calculation of the Liquid Velocity

Photos 1, 2, 3 and 4 are typical examples of the photographs of the horizontal plane (Z -view). In each photograph, the bold circular arc is the image of the streak of the spot-light from the pin-hole and the other fine spiral trajectories (both dotted and full lines) represent the images of the streaks of the gleaming particles. When the liquid velocity is comparatively high, the dotted-line streaks are obtained as shown in Photos 3 and 4, the dot's interval corresponds to a period of time of 1/120 second, because the light-source (mercury lamp) flickers 120 times per second corresponding to the cycles of the alternating current (60~). On the other hand, when the liquid velocity is slow, full-line streaks are obtained as shown in Photo 1. Photo 5 is an example of the view of the vertical plane (R -view) and the flow patterns of the liquid can be observed.

i) A-method

When the dotted-line streaks are obtained, as shown in Photo 3, 4 and a part of Photo 2, the liquid velocities are calculated by the method explained in Fig. 3(a) (let us call this the A-method), that is, the resultant velocity of the liquid on the horizontal plane is

$$v \doteq \frac{120l}{m} \tag{1a}$$

where m is the number of flickers of the mercury lamp and l is the length

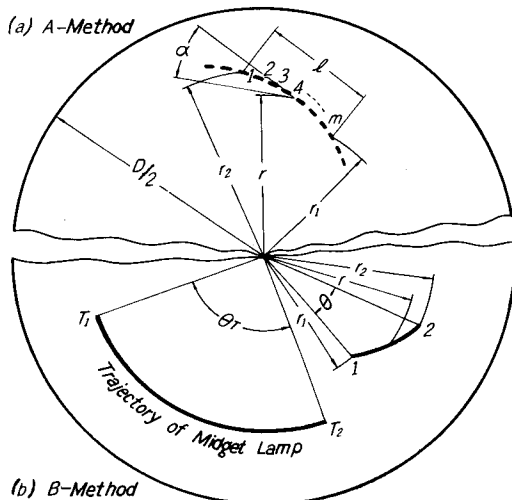


Fig. 3. Measurement of Velocity by the Photographic Method.

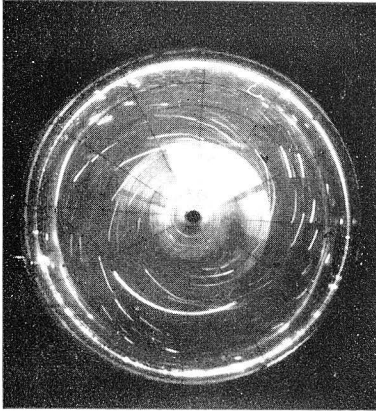


Photo 1

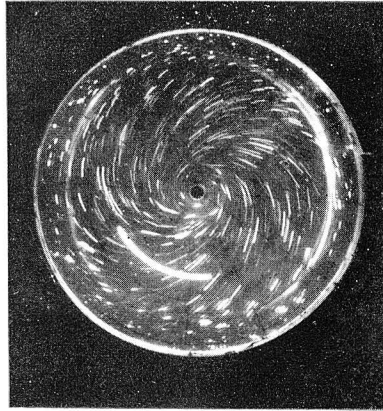


Photo 2

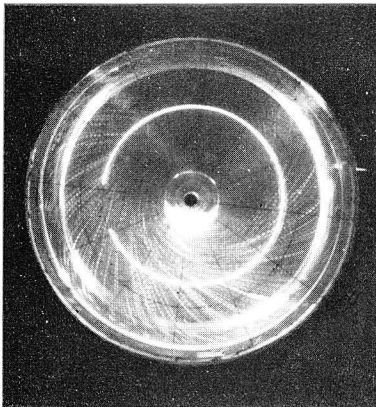


Photo 3

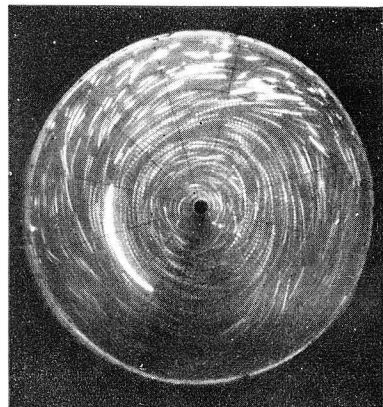


Photo 4

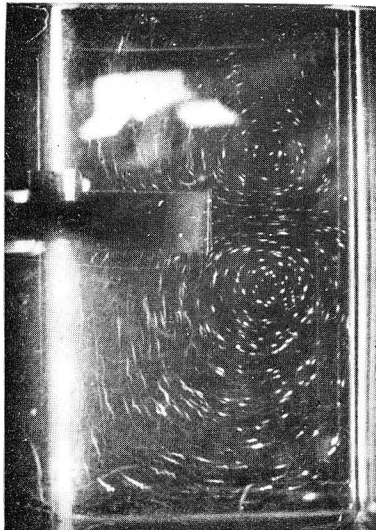


Photo 5

“Photographs of the Flow Patterns
for 8-Flat-Blade Paddle”

- Photo 1 $Re=14$, Exposure: 1/2 sec.
 $Z=-1.5$ cm, $N=30$ r.p.m.,
 $\rho=1.33$ g/cm³, $\mu=10.8$ poise
- Photo 2 $Re=89$, Exposure: 1/10 sec.
 $Z=-12$ cm, $N=108$ r.p.m.,
 $\rho=1.33$ g/cm³, $\mu=5.95$ poise
- Photo 3 $Re=89$, Exposure: 1/2 sec.
 $Z=-0.5$ cm, $N=108$ r.p.m.,
 $\rho=1.33$ g/cm³, $\mu=5.95$ poise
- Photo 4 $Re=1,200$, Exposure: 1/10 sec.
 $Z=-12$ cm, $N=108$ r.p.m.,
 $\rho=1.22$ g/cm³, $\mu=0.41$ poise
- Photo 5 $Re=55$, Exposure: 1 sec.
 $N=60$ r.p.m., $\rho=1.33$ g/cm³,
 $\mu=5.4$ poise

of the particle streak corresponding to the period of m -flickers. Concerning the angle α between the velocity v and the tangent to the circumference, the following relation is obtained.

$$\sin \alpha \doteq \frac{\Delta r}{l} = \frac{r_2 - r_1}{l}. \quad (1b)$$

Accordingly, the circumferential and radial components of the liquid velocity are

$$\left. \begin{aligned} v_t &= v \cdot \cos \alpha \\ v_r &= v \cdot \sin \alpha. \end{aligned} \right\} \quad (1c)$$

All these values are the velocities at the radial distance $r = \frac{r_2 + r_1}{2}$. In the present experiments, the values of $\Delta r = r_2 - r_1$ were between 0.3 cm and 0.75 cm.

ii) B-method

When the full-line streaks are obtained, as shown in **Photo 1** and partly in **Photo 2**, the liquid velocities are calculated by the method explained in **Fig. 3 (b)** (let us call this the B-method), that is,

$$v \doteq \frac{2\pi n}{\theta_T} \cdot L \quad (2a)$$

$$\sin \alpha \doteq \frac{\Delta r}{L} = \frac{r_2 - r_1}{L} \quad (2b)$$

$$\left. \begin{aligned} v_t &= v \cdot \cos \alpha \quad \text{or} \quad v_t = 2\pi r n \frac{\theta}{\theta_T} \\ v_r &= v \cdot \sin \alpha \end{aligned} \right\} \quad (2c)$$

where θ_T is the rotation angle of the impeller during the time of exposure and is equal to the visible angle of the spot-light streak about the center. L is the length of the particle streak and θ is the visible angle of the particle streak L about the center.

In the B-method, the measurement of the velocity should be confined only to the particles, which are present in the illuminated plane throughout the time of exposure, and should not include the particles which are leaving or entering. The particles that have entered or left the illuminated plane during that period can easily be distinguished, because the extremities of their paths are very obscure and they must be eliminated from consideration.

The B-method can also be applied to the case of the dotted-line streaks.

3) Reliability of this Photographic Method

Concerning the photographic method mentioned above, several considerations were made.

i) Unavoidable error accompanying this method

The velocity obtained by this method is the mean value for the width of the

illuminated plane and the distance Δr , which is naturally different from the case of pitot-tube method. If the width of the illuminated plane or the distance Δr is small, then the error due to the above reason decreases, but the reading error caused by measuring the streak length increases and, consequently, there is a considerable error in any case (perhaps 5~10% error in this experiment).

Furthermore, as mentioned above, when one component of the liquid velocity (for example v_z in this case) is much smaller than the others, the correct measurement of that component is very difficult by this method.

ii) Errors caused by the approximate equations such as Eqs. (1a), (1b), (2a) and (2b).

In this experiment, these errors may be considered negligible.

iii) The degree to which the tracer particles follow the liquid motion

If the relative velocity between the agitated liquid and the tracer particles is not small, the results obtained by this photographic method are not reliable. Therefore, the degree to which the tracer particles follow the liquid motion is of essentially importance.

The equation of motion of a spherical particle in a liquid is expressed as follows,

$$\left. \begin{aligned} \frac{dv_p}{dt} + \beta v_p &= \gamma \frac{dv_F}{dt} + \beta v_F \\ \beta &= \frac{3\rho_F \nu}{4(\rho_p + \rho_F/2) \cdot d_p^2} C_x(Re^*) \cdot Re^* \end{aligned} \right\} \quad (3)^{3),4)}$$

where v_p, v_F = velocity of the particle and of the liquid, respectively,

ρ_p, ρ_F = density of the particle and of the liquid, respectively,

d_p = diameter of the particle,

$Re^* = \frac{d_p(v_F - v_p)}{\nu}$ = Reynolds number referring to the relative velocity,

$C_x(Re^*)$ = drag coefficient of the particle which is a function of Re^* ,

γ = a constant.

The degree to which a particle follows the liquid is represented by β , and $1/\beta$ is a measure of the particle's inertia.

According to the physical properties shown in **Table 2**, it is estimated, that $1/\beta$ is not larger than $1/10^3$ second and the vertical velocity of the tracer particle in the liquid due to buoyancy is about 0.01 cm/sec in the case of highly viscous millet-jelly, so that the error is negligible. But, in the case of dilute millet-jelly, $1/\beta$ is not larger than $1/10^2$ second and the vertical velocity is about 0.3 cm/sec. This means that the error is not negligible.

iv) Comparison of the results obtained by methods A and B

Generally, there is good agreement between the results obtained by the two methods as shown in Fig. 4 (a), if the time of exposure is long enough ($T \geq 1/10$ second). Fig. 4 (b) shows an example of a poor agreement between the two, where the time of exposure is too short. The magnitude of such error is approximately evaluated by

$$\epsilon = \frac{L-L'}{L} \times 100 = \frac{\theta-\theta'}{\theta} \times 100 \quad [\%],$$

as shown in Fig. 4 (c).

In short, too short a time of exposure should be avoided.

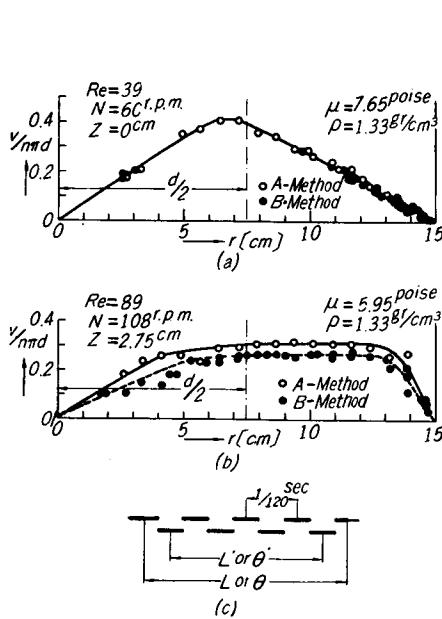


Fig. 4. Comparative Figures of Results Obtained by the A- and the B-Methods.

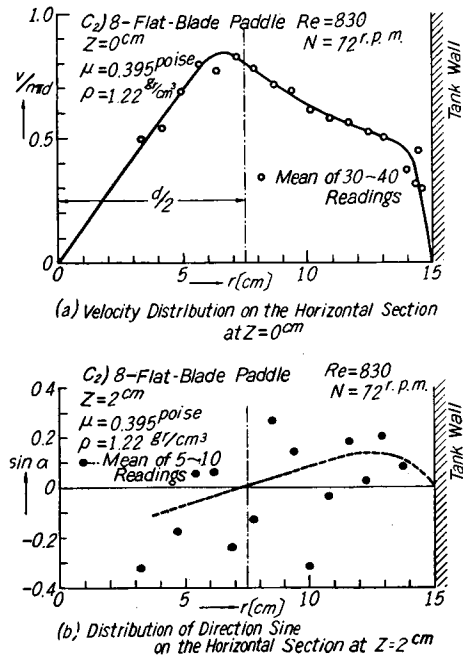


Fig. 5. Results Obtained in the Case of Turbulent Flow.

v) Measurement of turbulent liquid flow

In turbulent flow, the liquid velocity fluctuates at random about a mean value. Therefore, only a mean value obtained from numerous data gives a reliable value for the liquid velocity, as shown in Figs. 5 (a) and (b) for comparison. Furthermore, it is considered that the degree to which the tracer particle follows the motion of the liquid has a rather important effect on the reliability of the data.

Therefore, it is a very complicated and laborious task to measure the velocity of a turbulent fluid by the photographic method²⁾.

vi) Miscellaneous

The camera must be correctly set so that its optical axis is at right angles to the illuminated plane, otherwise the images on the photograph are distorted. Also the measurement of the streak length on the photograph must be made as accurately as possible.

It may be concluded that such a photographic method is suitable for the measurement of laminar fluid flow, especially when it is two-dimensional.

III. Results Obtained

As typical examples of the velocity distributions of an agitated liquid, the data obtained in the case of the 8-flat-blade paddle (refer to Table 1 (C_2)) are shown in Figs. 6 and 7. In Fig. 6, data calculated by the B-method are shown for the agitation at a comparatively low velocity.

Figs. 6 (a) and (b) show the distribution of the non-dimensional circumferential velocity ($v_t/n\pi d$) and $\sin \alpha$ at various radial positions and for several horizontal levels. It is obvious that the liquid velocity is rather high only in the neighbourhood of the impeller and decreases abruptly with the distance from the

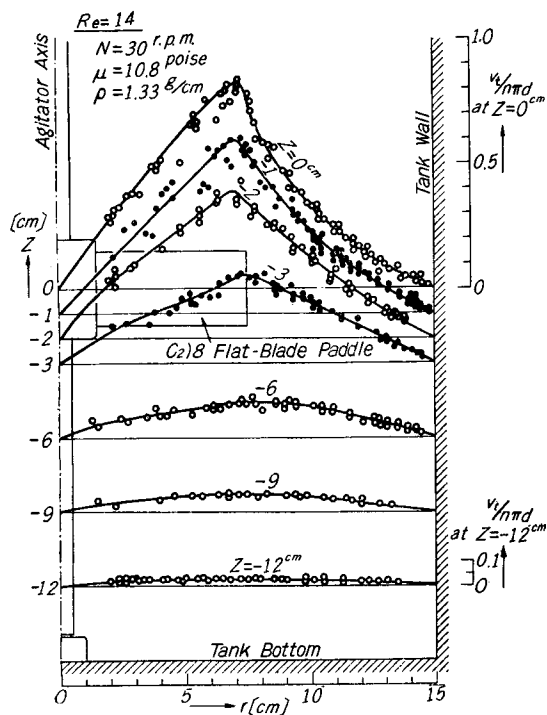


Fig. 6 (a). Distribution of $v_t/n\pi d$ at $Re=14$ for 8-Flat-Blade Paddle.

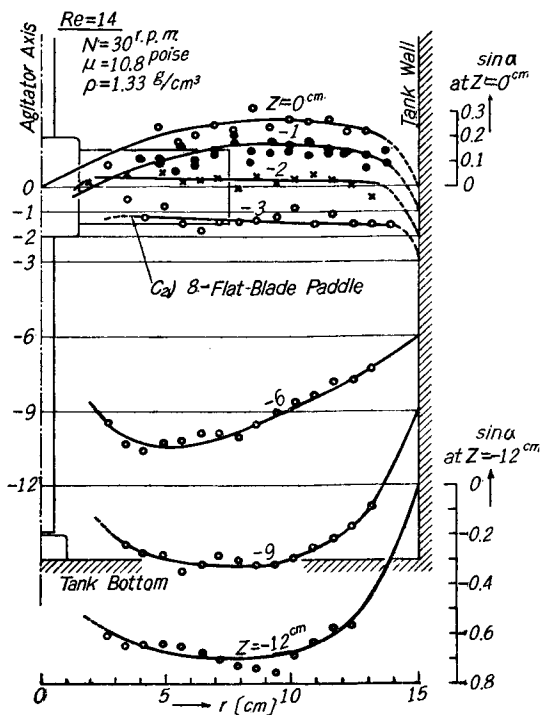


Fig. 6 (b). Distribution of $\sin \alpha$ at $Re=14$ for 8-Flat-Blade Paddle.

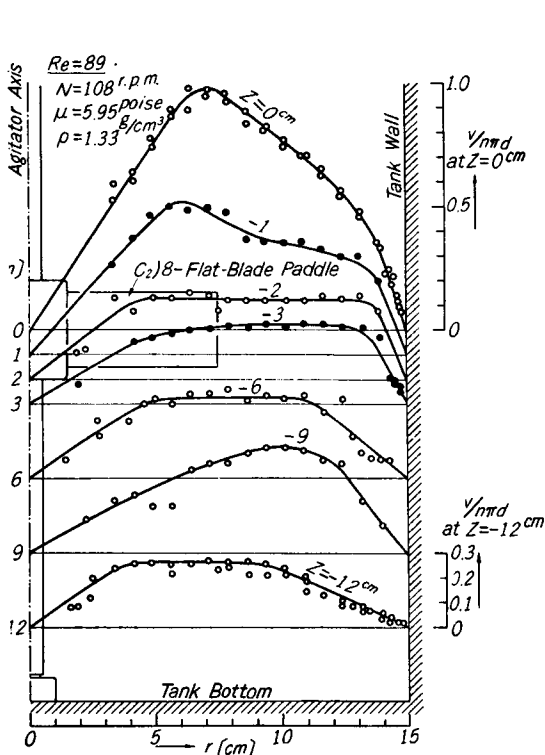


Fig. 7 (a). Distribution of $v/\pi nd$ at $Re=89$ for 8-Flat-Blade Paddle.

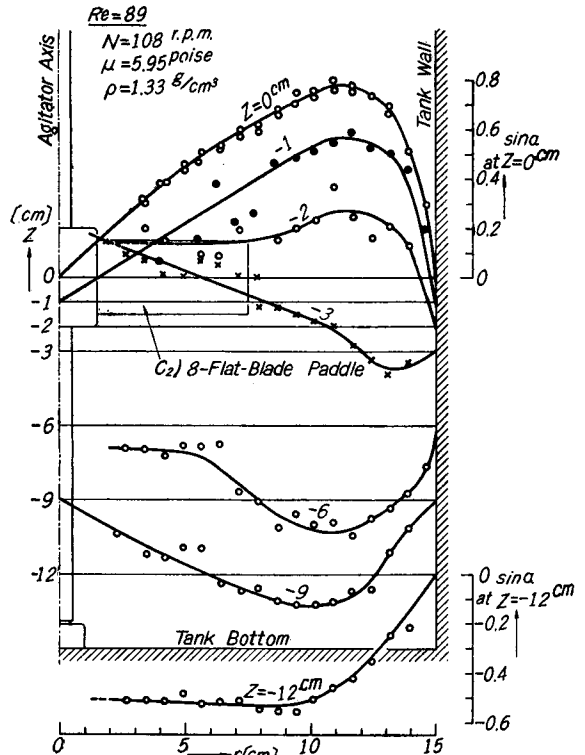


Fig. (b). Distribution of $\sin \alpha$ at $Re=89$ for 8-Flat-Blade Paddle.

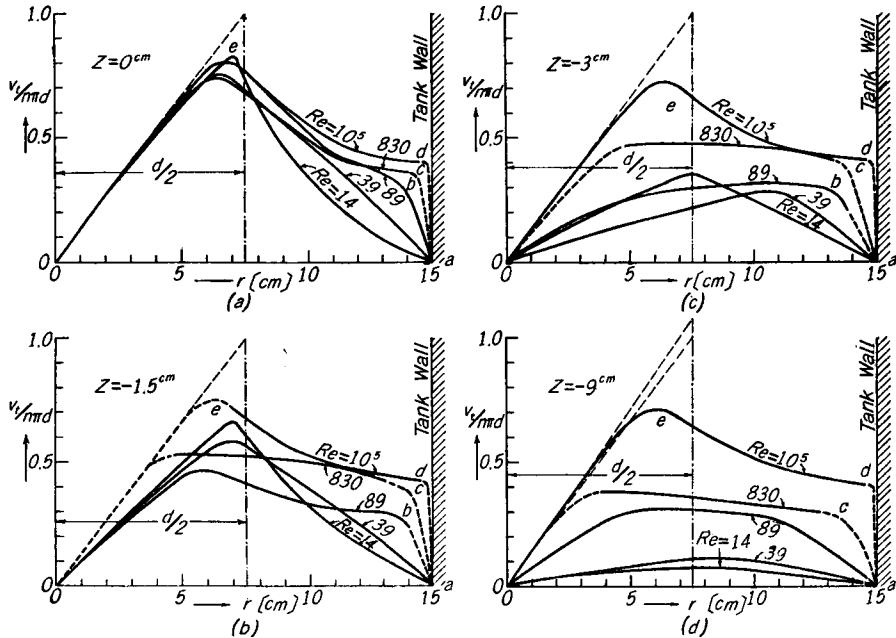


Fig. 8. Variation of Tangential Velocity Distribution with the Change in Reynolds Number at Various Horizontal Sections.

impeller. Similarly, the data calculated mainly by the A-method at a comparatively high agitator speed are shown in **Figs. 7 (a) and (b)**. From these data, the two components of liquid velocity v_t and v_r are calculated using Eqs. (1c) and (2c). **Figs. 8 (a), (b), (c) and (d)** show how the distribution of circumferential velocity ($v_t/n\pi d$) at various radial positions varies with the change in Reynolds number, for several horizontal levels, as well as some other data for completely turbulent fluid flow at $Re=10^5$ which were obtained by using pitot-tubes¹⁾. **Fig. 8 (a)** shows the velocity distribution at the midpoint of the liquid depth $z=0$ cm. As shown by the diagram, the variation of the velocity with Reynolds number is very small within the blade length (i.e. $r \leq 7.5$ cm), but very marked between the tip of the blades and the vessel wall (i.e. $7.5 \text{ cm} \leq r \leq 15$ cm). At a very low Reynolds number (for example $Re=14$) the velocity distribution in the outer region corresponds to that of laminar flow around a vortex (or a rotating solid such as a cylinder)²⁾, but, as Reynolds number increases, the velocity ($v_t/n\pi d$) becomes higher and the profile of the velocity distribution swells out as shown by \widehat{abe} , \widehat{ace} or \widehat{ade} , and at a high Reynolds number (for example $Re=830$ or 10^5), the liquid flow gets to be turbulent and the velocity distribution is similar to that in the potential flow region of Rankin's compound vortex. At points removed from the impeller, the liquid velocity is very low at low Reynolds number and becomes higher as Reynolds number increases, as shown in **Fig. 8 (d)**. At a very high Reynolds number, there is little difference between the velocity in the neighbourhood of the impeller and that at a distance, as **Figs. 8 (a), (b), (c) and (d)** clearly show. The laminar boundary layers at the vessel wall, which are shown in **Fig. 8** by \widehat{ab} , \widehat{ac} and \widehat{ad} , become thinner as Reynolds number increases.

The centrifugal force caused by the rotation of the impeller gives rise to a radial flow from the tip of the impeller blades towards the vessel wall, so that a secondary circulation flow occurs as shown in **Fig. 9** and **Photo 5**. **Figs. 10 (a), (b) and (c)** show how the distribution of radial velocity $v_r/n\pi d$ at different heights varies with the change in Reynolds number. Positive values indicate an outward flow from the axis to the vessel wall and negative values indicate an inward flow. The outward flow near the impeller blades has a broad width and a low velocity at a low Reynolds number, but the width narrows and the velocity rises, that is, the profile of the velocity distribution becomes more and more sharp, as Reynolds number increases. These phenomena mean that the liquid flow changes from laminar to turbulent. Especially, in the velocity distribution at $Re=89$, the sharp part of the velocity profile as shown by \widehat{bab} is in distinct contrast with the smooth part of the velocity profile as shown by \widehat{bc} . The former

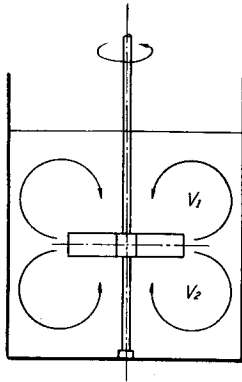


Fig. 9. Secondary Circulation Flow.

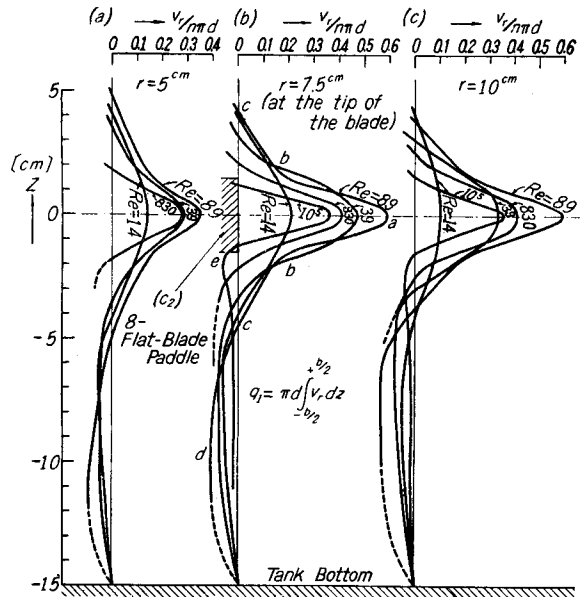


Fig. 10. Variation of Radial Velocity Distribution with the Change in Reynolds Number at Various Radial Positions.

indicates that the liquid flow is turbulent, while the latter is laminar. Therefore, it is obvious that both laminar and turbulent flow exist at the same time in the vessel in these ranges of Reynolds number. In other words, the liquid flow in the vessel is in the state of so-called transitional flow. As Reynolds number increases, the turbulent state propagates from the liquid near the impeller to the whole liquid in the vessel. The discharge flow or the secondary circulation flow is considerably more intense in the transitional flow range compared with that in the laminar or turbulent flow range, as shown in Fig. 10. In the completely turbulent flow range, the width of the discharge flow at the tip of the blades is narrower than the width of the impeller blade and there is a strong suction flow near the corners of blade tips.

IV. Comparison of the Results Obtained

1) Velocity Distribution and Secondary Circulation Flow

As mentioned in the preceding section in reference to Figs. 8 and 10, there was a very large difference between the liquid velocity near the impeller and removed from the impeller at low Reynolds number. As Reynolds number increases, this difference becomes smaller and the liquid velocity distribution is considerably unified throughout the liquid in the vessel. These phenomena are clearly

indicated in Fig. 11, and may be explained as follows. At very low Reynolds number, there is no turbulent flow and the secondary circulation flow is very weak, so that the momentum transfer from the liquid near the impeller to the more remote parts of the liquid depends mainly upon the molecular viscosity of the liquid, and therefore the amount transferred is small and the velocity of remote liquid is low. As Reynolds number increases, secondary circulation flow occurs and the momentum transfer increases. At high Reynolds number, turbulent flow occurs and momentum transfer by the turbulent viscosity becomes predominant. Thus the liquid velocity distribution is considerably unified. In the turbulent flow range, though the momentum transfer caused by the secondary circulation is comparatively small, it may have some influence on the profile of the velocity distribution and often performs a very important role in the mixing of the liquid in the vessel.

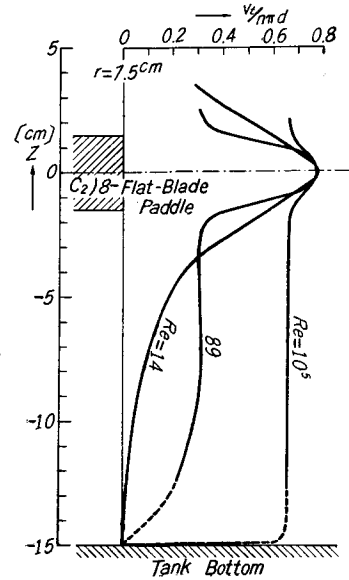


Fig. 11. Variation of Tangential Velocity Distribution with the Change in Reynolds Number at $r=7.5$ cm.

2) Discharge Performance and Characteristic Curves

Concerning the discharge performance of the impellers, the discharge flow rate from the tip of the impeller blades q_1 or its non-dimensional representation (coefficient of discharge) $N_{q_1} = q_1/n\pi d^3$, and the ratio of the power number N_P and the coefficient of discharge N_{q_1} , (N_P/N_{q_1}), are adopted, as in the previous report¹⁾. The discharge flow rate q_1 is calculated by the following equation,

$$q_1 = \pi d \int_{-b/2}^{+b/2} v_r dz \quad (4)$$

from the data on the radial velocity distribution at the tip of the blades as shown in Fig. 10 (b).

Values of N_P , N_{q_1} and N_P/N_{q_1} are shown in Table 3 for various Reynolds number and different impellers. Fig. 12 shows the relations between N_P , N_{q_1} or N_P/N_{q_1} and Reynolds number Re , that is, the characteristic curves of an impeller concerning power consumption and discharge performance.

Since many discussions have already been made on the characteristics of the power consumption of an agitating impeller, further explanations are omitted here.

Table 3. Discharge Performance of Various Impellers.

Impeller	Re[-]	N[r.p.m.]	ρ [gr/cm ³]	μ [poise]	N_P [-]	N_{q1} [-]	N_P/N_{q1} [-]
C_2 8-Flat-Blade Paddle	6.7	25	1.35	16.7	17	0.28	61
	14	30	1.33	10.8	9.4	0.37	25
	39	60	"	7.65	5.1	0.80	6.4
	89	108	"	5.95	4.05	0.86	4.7
	830	72	1.22	0.395	2.2	0.57	3.9
	10 ⁵	72	1.00	0.01	0.95	0.34	2.8
b' 8-Flat-Blade Turbine	17	30	1.33	8.6	7.0	0.42	17
	38	60	"	7.9	4.5	0.58	7.8
	84	120	"	7.1	3.5	0.62	5.7
	630	72	1.22	0.52	2.1	0.60	3.5
	10 ⁵	72	1.00	0.01	0.93	0.34	2.7
d_2 8-Retreated-Blade Paddle	23	30	1.33	6.6	5.1	0.45	11.3
	43	60	"	7.0	3.9	0.65	6.0
	78	120	"	7.7	3.2	0.67	4.8
	700	72	1.22	0.47	1.6	0.63	2.5
	10 ⁵	72	1.00	0.01	0.71	0.43	1.7

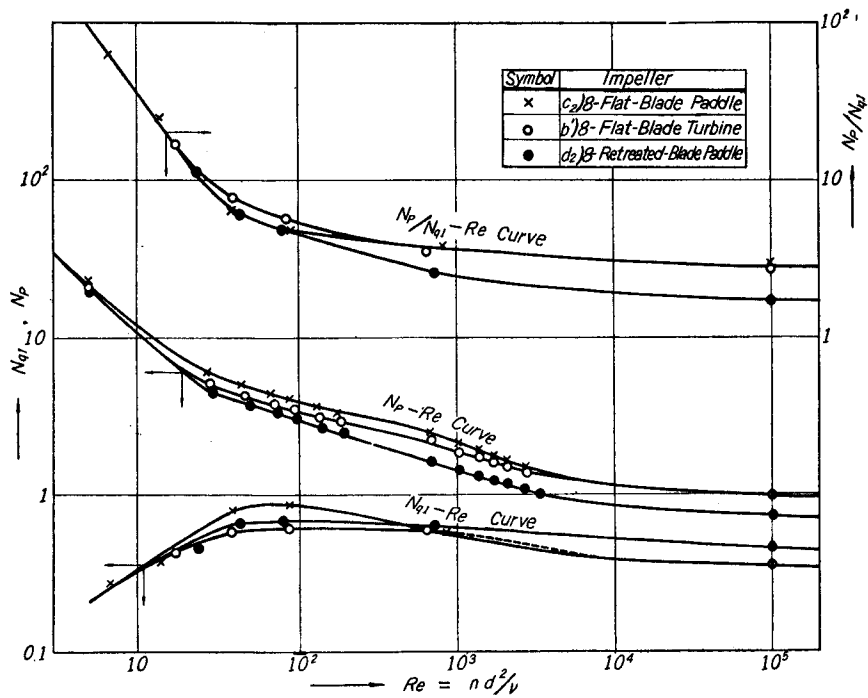


Fig. 12. Characteristic Curves for Various Types of Impellers.

The characteristics curve for the discharge capacity ($N_{q_1}-Re$ curve) shows the following facts. All types of impeller have poor discharging capacity in the very low Reynolds number range ($Re < 10$). In the transitional flow range, all the impellers, especially the flat-blade paddle, show a comparatively large discharge capacity, but in the turbulent flow range the discharge capacity decreases again to some extent. Therefore, a maximum value of N_{q_1} exists in the transitional flow range. These trends are conspicuous for the flat-blade paddle which has high form drag, whereas the retreated-blade paddle which has low form drag shows a larger capacity than the others in the turbulent flow range, as already mentioned in the previous report¹⁾. These phenomena suggest that there are close interrelations between the type of impeller, its discharge capacity and the flow conditions of the liquid caused by the rotation of the impeller, especially in the range of transitional flow. For example, by the attachment of a circular disc to the impeller blades as is the case of the turbine type, or by the retreatment of the impeller blades, the transition of the liquid flow from the laminar to the turbulent state is suppressed to some extent.

The characteristic curve for the discharge efficiency ($N_P/N_{q_1}-Re$ curve) shows that all types of impellers have almost equal discharge efficiency in the range of low Reynolds number but that the retreated-blade paddle is best in the turbulent flow range. The turbine type impeller has no remarkable features as far as these characteristics are concerned.

3) Considerations on the Relation between the Characteristic Curves and the State of Liquid Flow

As mentioned above, the characteristic curves of an impeller and the liquid flow conditions are closely connected each other. Let the general relations be considered.

Fig. 13 shows the schematic diagram of the characteristic curves for several impellers. The curve representing the relation between N_P and Re shows that the power number N_P decreases in inverse proportion to the increase of Reynolds number, as shown by the straight line \overline{ab} , in the range of very low Reynolds number \overline{AB} . In this region, the secondary circulation flow is very

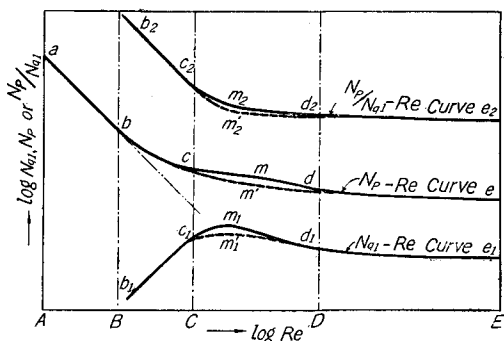


Fig. 13. Schematic Diagram of Characteristic Curves.

weak and negligible, and the liquid motion is very slow except near the impeller as mentioned above. In the \overline{BC} range of Reynolds number, where the liquid flow is also laminar but the secondary circulation flow grows gradually as shown by $\overline{b_1c_1}$, the tendency of the power number N_P to decrease becomes less as shown \overline{bc} . As Reynolds number increases further, turbulent flow occurs in the liquid near the impeller and gradually propagates to the whole liquid. Thus, in the transitional range \overline{CD} , the discharging capacity N_{q_1} exhibits a maximum value as shown by m_1 or m'_1 , which corresponds to the value for an impeller having comparatively high form drag like the flat-blade paddle or an impeller having lower form drag like the retreated-blade paddle, respectively, as already mentioned in the preceding paragraph. Correspondingly, the characteristic curves of N_{q_1} and N_P are shown by the swelled out curves $\widehat{c_1m_1d_1}$ and \widehat{cmd} or by the smoother curves $\widehat{c_1m'_1d_1}$ and $\widehat{cm'd}$. Therefore, it is supposed that the shape of these curves represents the rate of transition from laminar to turbulent flow.

In the turbulent flow range \overline{DE} , there are many studies concerning the power consumption of impellers and the flow patterns of agitated liquid, therefore such discussions may be omitted.

The characteristics curve of the ratio N_P/N_{q_1} , which represents the power consumption required for a unit quantity of discharge flow rate, is necessarily determined by the two characteristic curves of N_P and N_{q_1} .

Based upon these discussions, if the characteristics curve of the power consumption ($N_P - Re$ relation) for an impeller is known, then the flow characteristics of the agitated liquid in the vessel may be estimated approximately.

V. Conclusions

The flow patterns of agitated liquids in a cylindrical vessel and the discharge performance of three typical impellers were measured for the laminar and transitional flow range, and combined with the results obtained in the previous report for the turbulent flow range, the characteristics curves for $N_P - Re$, $N_{q_1} - Re$ and $N_P/N_{q_1} - Re$ were drawn. The types of flow of the agitated liquid over a wide range of Reynolds number were also discussed. Especially, various phenomena in the transitional flow range which were hitherto unknown, that is, the outlines of the transition from laminar to turbulent flow and its relation to the shapes of the characteristic curves were made clear.

Nomenclature

b	= Width of impeller blades	[cm]
D	= Tank diameter	[cm]
d	= Impeller diameter	[cm]
g_c	= Gravitational conversion factor	[g·cm/G·sec ²]
H	= Liquid depth	[cm]
H_p	= Height of the impeller from the tank bottom	[cm]
L	= Length of particle streak (refer to Fig. 3 (b))	[cm]
l	= Length of particle streak corresponding to the period of m -flickers	[cm]
m	= Number of flickers of mercury lamp	[—]
N	= Impeller speed in r.p.m.	[1/min.]
n	= Impeller speed in r.p.s.	[1/sec.]
n_p	= Number of impeller blades	[—]
$N_p = P \cdot g_c / \rho n^3 d^5$: Power number	[—]
$N_{q_1} = q_1 / n \cdot d^3$: Coefficient of discharge	[—]
P	= Power consumption of the impeller	[G·cm/sec.]
q_1	= Discharge flow rate from the tip of impeller blades	[c.c./sec] or [liters/sec]
r	= Radial position from the agitator axis	[cm]
$Re = n \cdot d^2 / \nu$: Modified Reynolds number	[—]
T	= Time of exposure	[sec.]
V	= Resultant velocity of liquid	[cm/sec.]
v	= Resultant velocity of liquid on a horizontal plane	[cm/sec.]
v_t	= Circumferential component of liquid velocity	[cm/sec.]
v_r	= Radial component of liquid velocity	[cm/sec.]
v_z	= Vertical component of liquid velocity	[cm/sec.]
z	= Height from the midpoint of liquid depth	[cm]
α	= Angle between the velocity v and the tangent to the circumference on a horizontal plane (refer to Fig. 3)	[—]
μ	= Viscosity of liquid in poise	[g/cm·sec.]
$\nu = \mu / \rho$: Kinematic viscosity of liquid	[cm ² /sec.]
θ	= Visible angle of particle streak L about the center (refer to Fig. 3 (b))	[—]
θ_T	= Rotation angle of the impeller during time of exposure	[—]
ρ	= Density of liquid	[g/cm ³]

References

- 1) S. Nagata, K. Yamamoto and M. Ujihara; This memoirs, 20 No. 4 p. 336~349 (Oct. 1958).
- 2) J. P. Sachs and J. H. Rushton; Chem. Eng. Prog., 50 p. 597~603 (1954).

- 3) S. K. Friedlander; *A. I. Ch. E. Jour.*, **3** p. 381~385 (1957).
- 4) A. B. Basset; "A Treatise on Hydrodynamics" Vol. II, p. 285 (Cambridge 1888).
- 5) W. Müller; "Einführung in die Theorie der zähen Flüssigkeiten" S. 203 (Akad. Verlags. 1932).